AIAA JOURNAL
Vol. 43, No. 9, September 2005

Performance of a Shock Tube with a Large-Area Contraction

George Emanuel,* U. S. Satyanand,† and Frank K. Lu‡
University of Texas at Arlington, Arlington, Texas 76019

An inviscid, analytical model is provided for shocktube performance when there is a large, abrupt contraction in the low-pressure side of a tube. The analysis is independent of initial high-pressure side conditions. Only the ratio of specific heats of the low-pressure gas, the large-diameter tube's incident shock Mach number, and the contraction ratio are needed for a nondimensional solution of the transmitted flow in the small-diameter tube. This solution is unique, readily evaluated, and various limits and constraints are discussed. Parametric calculations establish the increased magnitude of the transmitted shock Mach number relative to the shock Mach number for a tube without contraction. The Mach number increase, then increases the pressure and temperature downstream of the small-diameter tube's incident and reflected shocks, again relative to a tube without a contraction. Shock-tube performance, therefore, can be improved by the addition of a small-diameter tube to an existing tube's low-pressure side. The improvement can be used with a combustion-driven tube, a free-piston tube, etc.

Nomenclature

A	=	cross-sectional area
a	=	speed of sound
J_+	=	C_+ Riemann invariant
M	=	Mach number
p	=	pressure
R	=	gas constant
$\bar{R}$	=	universal gas constant
s	=	entropy
T	=	temperature
W	=	molecular weight
w	=	flow speed
X	=	$1 + [(\gamma - 1)/2]M^2$
Y	=	$\gamma M^2 - (\gamma - 1)/2$
Z	=	$M^2 - 1$
α	=	contraction ratio, A_L/A_R
γ	=	ratio of specific heats
ρ	=	density

Subscripts

L	=	left side of contraction
R	=	right side of contraction
r	=	reflected shock wave
s	=	incident shock in the large-diameter tube
t	=	incident transmitted shock
0	=	stagnation
1, 2, . . . , 10	=	flow states or regions

Superscript

(1)	=	first estimate

Introduction

THE low-pressure side of a shock tube is sometimes modified from its usual closed-end configuration. Modifications include a Ludwieg tube[1,2] or a shock tunnel.[3] Another modification is an abrupt, large contraction in the low-pressure side that leads into a small-diameter tube with a closed end. Adding a small-diameter tube to an existing facility is simple and cost effective. Moreover, it does not conflict, for example, with free-piston or combustion-driven operation. A sudden contraction increases the transmitted shock Mach number M_t relative to the large-diameter tube's incident shock Mach number M_s. In turn, this increases the pressure, temperature, and Mach number, M_8, in the gas downstream of the transmitted shock. Moreover, the pressure and temperature behind the reflected shock in a small-diameter tube can significantly exceed that behind the reflected shock in the closed end of a large-diameter tube. In addition to the preceding, a variety of approaches have been used to improve the performance of shock tubes.[4] These include increasing the pressure or temperature of the driver gas, using a light driver gas, or using expansion, free-piston, combustion or detonation drivers.[3–17] A further increase in performance can be achieved by combining these techniques with an area contraction.

The facilities just highlighted, however, were without the benefit of a contraction to further increase the temperature in the reflected shock gas region. In general, the temperature, or enthalpy, in a small-diameter tube's reflected shock region can exceed by about 50% that in a large-diameter tube's reflected shock region. A contraction is thus beneficial for radiative heat transfer, chemical kinetic, and plasma studies, as well as for shock-tunnel operation. Moreover, it can be used in combination with other performance enhancing techniques, such as a light driver gas.

A sudden or a gradual contraction of the tube at the diaphragm section also increases the incident shock Mach number. Alpher and White[18] provide an inviscid analysis for a gradual monotonic convergence of the tube in the diaphragm section. Nonideal diaphragm rupture, however, complicates flow behavior and results in a different and more complex model than the one discussed here. Operationally, this approach is more involved than a low-pressure side contraction.

Salas[19] provides an analysis for an abrupt area change, either expanding or contracting, away from the diaphragm and in the low-pressure side of the tube. The analysis, however, is limited to a small area change. In this circumstance, a multiplicity of solutions is possible, and the computational procedure utilizes an involved iteration. Both the Alpher and White[18] and Salas[19] analyses are one dimensional, that is, they model flow conditions along the axis of the tube, as is the case in the present study. By limiting the area contraction to a relatively large value, say two or more, a unique solution is obtained. The iterative procedure of Salas[19] is also removed.

Standard assumptions are utilized for the inviscid analysis of an idealized shock-tube flow. Perfect, possibly different, gases are used in the high- and low-pressure sections. The analysis for incident flow conditions in the large-diameter tube is well known[20] and is

Received 11 August 2004; revision received 13 April 2005; accepted for publication 21 April 2005.

*Professor, Department of Mechanical and Aerospace Engineering. Associate Fellow AIAA.

†Graduate Research Associate, Department of Mechanical and Aerospace Engineering.

‡Professor and Director, Aerodynamics Research Center, Department of Mechanical and Aerospace Engineering. Associate Fellow AIAA.

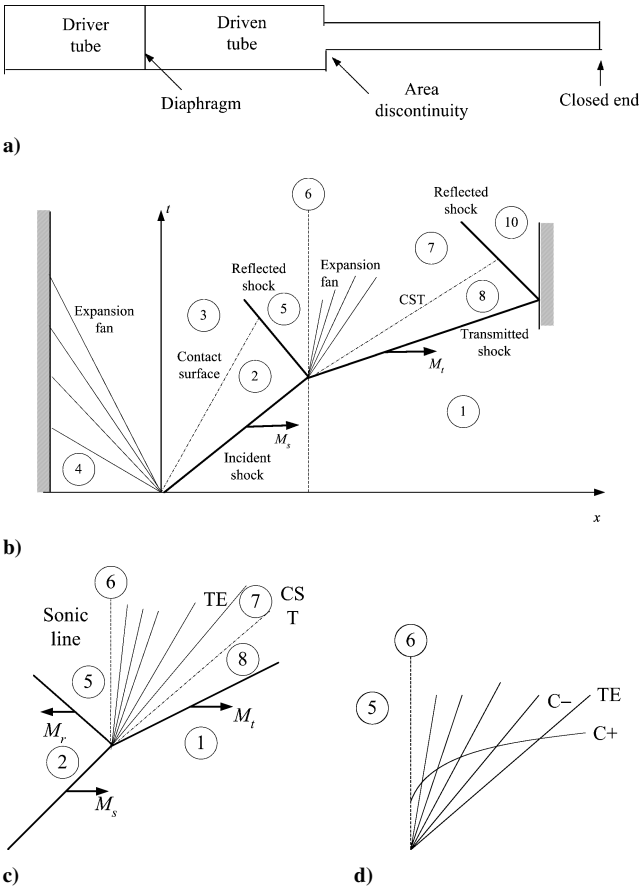

Fig. 1 Configuration and wave diagram for a shock tube with a large-area contraction in the driven section: a) schematic, b) idealized wave diagram, c) wave diagram in the vicinity of the contraction, and d) wave diagram for the rarefaction.

not reproduced. The temperature T_1, pressure p_1, molecular weight W, and ratio of specific heats γ of the gas in the low-pressure side of the tube are presumed known, as is the Mach number M_s for the incident shock in the large-diameter tube (see Fig. 1). As a consequence, values for γ_4, W_4, T_4, and p_4 for the high-pressure gas are unnecessary. The subsequent analysis thus terminates before flow conditions, associated with the high-pressure gas, alter the flow associated with the contraction. Along with T_1, p_1, γ, W, and M_s, the only other specified parameter is the contraction area ratio α.

Pressure, temperature, and density are normalized by their state 1 values, and flow speeds are normalized by the speed of sound in state 1, a_1. A nondimensional solution is only a function of γ, M_s, and α. For instance, these parameters are sufficient to establish the transmitted shock Mach number M_t. Relations are provided for flow conditions of the gas between the transmitted shock and the contact surface in the small-diameter tube and for conditions behind the reflected shock. This surface stems from the wave reflection process that starts at the contraction. Results are developed under the assumption of a large contraction ratio, that is, $\alpha \gg 1$. Later analysis shows that there is relatively little benefit associated with a contraction when α is in excess of about 5.

A novel analytical model is presented in the next section. The last section outlines parametric calculations and briefly summarizes results.

Analysis

Preliminary Remarks

The overall model is described before key features are discussed. Figure 1 contains a schematic and wave diagrams for idealized shock-tube flow with an abrupt, large contraction in the driven section. Regions 1 and 4 contain the initial low- and high-pressure gases in the driven and driver sections, respectively. To the left of state 6, the cross-sectional area is A_L, and to the right it is A_R, where $\alpha = (A_L/A_R)$. The incident shock partly reflects from the contraction thereby giving rise to region 5. Part of the incident shock propagates into the small diameter tube with a Mach number M_t. Region 8 is a uniform flow region between the transmitted shock and the contact surface, labeled CST. Pressure and velocity tangency conditions apply across CST. Region 7 is also a uniform flow region. A rarefaction wave is required between states 6 and 7, where state 6 is sonic. This description is based on Salas,[18] who validates it using a quasi-one-dimensional time-dependent Euler code.

Figure 1c provides an enlargement of the flowfield in the vicinity of the contraction. In a closed-end shock tube, region 5 is quiescent. This is also the case for the gas at the outer tube wall, away from the opening. Gas, however, flows through the inlet of the small diameter tube. Consequently, the gas is not quiescent on the tube's axis, and M_5 has a small positive value, which stems from a positive flow speed w_5 just downstream of the inlet to the small-diameter tube. The reflected shock is thus strongest at its perimeter and slightly weaker on the tube's axis. The reflected shock, in the figure, is for the shock on the axis, where its Mach number is M_r.

The combination of incident and reflected shocks in the large-diameter tube is stronger than the transmitted shock. Hence, the pressure and specific entropy satisfy

$$p_5 > p_8, \qquad s_5 > s_8$$

The pressure inequality requires a rarefaction wave whose sonic leading edge is at state 6. The strength of the rarefaction is such that the pressure at its trailing edge (TE) matches the pressure just downstream of the transmitted shock. Because the entropy in regions 5, 6, 7 and throughout the rarefaction wave is the same, the entropy in region 7 exceeds that in region 8. These two regions are therefore separated by a contact surface labeled CST.

There is a limitation on the maximum strength of the transmitted shock because p_8 cannot exceed p_5. On the other hand, the M_s Mach number represents a lower bound for M_t because the transmitted shock cannot have this value, as it corresponds to a quiescent gas, on the axis, in region 5. The model thus bounds M_t, where the lower bound is M_s.

Validity of the model is based on Euler code[18] results. A self-consistent unique solution is obtained, and second-law violations are avoided. This means that the following entropy inequalities apply:

$$s_1 < s_2 < s_5, \qquad s_1 < s_8 < s_5$$

Region 5

Conservation of mass for a steady flow across the contraction yields

$$\alpha = A_L/A_R = (M_6/M_5)(X_5/X_6)^{(\gamma+1)/[2(\gamma-1)]} \tag{1}$$

where the X, Y, and Z Mach-number functions are defined in the Nomenclature. With $M_6 = 1$, this simplifies to

$$\alpha = (1/M_5)\{[2/(\gamma+1)]X_5\}^{(\gamma+1)/[2(\gamma-1)]} \tag{2}$$

Because α is prescribed, solve for M_5 to obtain

$$[(\gamma+1)/2](\alpha M_5)^{2(\gamma-1)/(\gamma+1)} - [(\gamma-1)/2]M_5^2 - 1 = 0 \tag{3}$$

When $\alpha = 1$, there is no contraction, regions 5–7 do not exist, region 8 is identical to region 2, and $M_t = M_s$. Equation (3), however, requires $M_6 = 1$ and yields $M_5 = 1$ when $\alpha = 1$. The model represents a different flowfield, compared to that with no contraction, and is therefore singular in the $\alpha = 1$ limit. At the other extreme, when $\alpha \ggg 1$, M_5 is nearly zero, and a first estimate is obtained by disregarding the M_5^2 term in Eq. (3):

$$M_5^{(1)} = [2/(\gamma+1)]^{(\gamma+1)/[2(\gamma-1)]}(1/\alpha) \tag{4}$$

This estimate differs from M_5 of Eq. (3) by less than 2.3% when $\alpha = 3$ and $\gamma = 1.4$. The difference further decreases as α increases.

The $\alpha \to \infty$ case results in a quiescent gas in region 5, which is also a singular limit for the model.

For a reflected shock, M_r and $\tilde{M}_r$ here denote a shock-fixed Mach number and a laboratory Mach number, respectively. Emanuel[21] [Eq. (12.25b)] provides a relation for a reflected shock in which the downstream flow is not necessarily quiescent. With the current notation, this relation is

$$M_5 = \frac{1 - [(\gamma+1)/2]\tilde{M}_r(M_2 + \tilde{M}_r) + [(\gamma-1)/2](M_2 + \tilde{M}_r)^2}{\left(\left\{1 + [(\gamma-1)/2](M_2 + \tilde{M}_r)^2\right\}\left[\gamma(M_2 + \tilde{M}_r)^2 - (\gamma+1)/2\right]\right)^{\frac{1}{2}}} \tag{5}$$

The single unknown is $\tilde{M}_r$ because M_2 is evaluated in the appendix and M_5 by Eq. (3). A first $\tilde{M}_r^{(1)}$ estimate is obtained by setting the numerator equal to zero:

$$\tilde{M}_r^{(1)} = \left\{1 + [(\gamma+1)/4]^2 M_2^2\right\}^{\frac{1}{2}} - [(3-\gamma)/4]M_2 \tag{6}$$

Starting with this value, $\tilde{M}_r$ is numerically established. The shock-fixed Mach number

$$M_r = M_2 + \tilde{M}_r \tag{7}$$

is used to establish the following region 5 properties:

$$p_5/p_1 = [2/(\gamma+1)]Y(M_r)(p_2/p_1) \tag{8a}$$

$$T_5/T_1 = [2/(\gamma+1)]^2\left[X(M_r)Y(M_r)\Big/M_r^2\right](T_2/T_1) \tag{8b}$$

$$a_5/a_1 = (T_5/T_1)^{\frac{1}{2}} \tag{8c}$$

where p_2/p_1 and T_2/T_1 are given in the Appendix.

State 6

The speed of sound at state 6 is established by the conditions

$$s_6 = s_5 \tag{9a}$$

$$M_6 = 1 \tag{9b}$$

$$T_{06} = T_{05} \tag{9c}$$

where T_0 is the stagnation temperature. Observe that the stagnation temperature relation is equivalent to an energy equation, and this means that the flow between regions 5 and 6 is viewed as steady. Equations (9a) and (9c), respectively, yield

$$p_6/p_5 = (T_6/T_5)^{\gamma/(\gamma-1)} \tag{10}$$

$$T_6/T_5 = X_5/X_6 \tag{11}$$

With Eq. (9b), the preceding reduces to

$$a_6/a_1 = \{[2/(\gamma+1)]X_5\}^{\frac{1}{2}}(a_5/a_1) \tag{12}$$

where M_5 and a_5/a_1 are given, respectively, by Eqs. (3) and (8c).

State 7

Conditions associated with state 7 require the theory of characteristics for a simple, centered rarefaction wave.[21] Figure 1d is a sketch of the rarefaction, where the C_- characteristics are straight, while curved C_+ characteristics connect states 6 and 7. The relevant equations are

$$s_7 = s_6 \tag{13a}$$

$$J_{+6} = J_{+5} \tag{13b}$$

where J_+ is a Riemann invariant:

$$J_+ = w + [2/(\gamma-1)]a \tag{14}$$

Equations (13b) and (14) yield

$$a_7\{1 + [(\gamma-1)/2]M_7\} = [(\gamma+1)/2]a_6 \tag{15}$$

and Eqs. (9a) and (13a) provide

$$p_7/p_5 = (T_7/T_5)^{\gamma/(\gamma-1)} = (a_7/a_5)^{2\gamma/(\gamma-1)} \tag{16}$$

M_t* and *a_7/a_1

The CST surface requires

$$p_8 = p_7 \tag{17a}$$

$$w_8 = w_7 \tag{17b}$$

The incident shock in the small-diameter tube yields

$$p_8/p_1 = [2/(\gamma+1)]Y_t \tag{18a}$$

or

$$M_t = \left((1/\gamma)\{[(\gamma+1)/2](p_8/p_1) + (\gamma-1)/2\}\right)^{\frac{1}{2}} \tag{18b}$$

With the aid of Eqs. (16) and (17a), p_8/p_1 can be eliminated with

$$p_8/p_1 = (p_7/p_5)(p_5/p_1) = (a_7/a_5)^{2\gamma/(\gamma-1)}(p_5/p_1) \tag{19}$$

where p_5/p_1 is given by Eq. (8a). The preceding two equations combine to yield

$$\gamma M_t^2 - \frac{\gamma+1}{2}\frac{p_5/p_1}{(a_5/a_1)^{2\gamma/(\gamma-1)}}\left(\frac{a_7}{a_1}\right)^{2\gamma/(\gamma-1)} = \frac{\gamma-1}{2} \tag{20}$$

whose unknowns are M_t and a_7/a_1.

A second equation for M_t and a_7/a_1 is developed starting from Eq. (15). First, M_7 is eliminated with

$$w_8/a_1 = [2/(\gamma+1)][Z(M_t)/M_t] = w_7/a_1 \tag{21}$$

$$M_7 = (w_7/a_1)(a_1/a_7) = [2/(\gamma+1)][Z(M_t)/M_t](a_1/a_7) \tag{22}$$

Equation (15) thus becomes

$$a_7/a_1 + [(\gamma-1)/(\gamma+1)][Z(M_t)/M_t] = [(\gamma+1)/2](a_6/a_1) \tag{23}$$

where a_6/a_1 is given by Eq. (12). Equations (20) and (23) are two coupled equations for M_t and a_7/a_1, where

$$1 < M_s < M_t \tag{24}$$

The a_7/a_1 parameter can be eliminated, but this was not done because the coupled equations are readily solved numerically. Once M_t and a_7/a_1 are established, M_7 is given by Eq. (22).

Region 8

The state of the gas in region 8 is given by

$$p_8/p_1 = [2/(\gamma+1)]Y_t \tag{25a}$$

$$T_8/T_1 = [2/(\gamma+1)]^2\left(X_tY_t\Big/M_t^2\right) \tag{25b}$$

$$\rho_1 = p_1/RT_1 \tag{25c}$$

$$\rho_8/\rho_1 = [(\gamma+1)/2]\left(M_t^2\Big/X_t\right) \tag{25d}$$

$$M_8 = Z_t/(X_tY_t)^{\frac{1}{2}} \tag{25e}$$

$$a_8/a_1 = (T_8/T_1)^{\frac{1}{2}} \tag{25f}$$

$$w_8/a_1 = (a_8/a_1)M_8 \tag{25g}$$

$$w_t/a_1 = M_t \tag{25h}$$

Table 1 Parametric M_s results when $\gamma = 1.4$ and $\alpha = 5$

										p_4/p_1		
M_s	M_t	M_2	M_8	p_2/p_1	p_8/p_1	T_2/T_1	T_8/T_1	w_2/a_1	w_8/a_1	Air/air	Helium/air	Helium/argon
2.5	2.891	1.197	1.327	7.130	9.580	2.138	2.553	1.750	2.121	145.3	21.56	18.75
3.0	3.478	1.358	1.467	10.33	13.94	2.679	3.284	2.222	2.658	632.6	44.21	35.93
3.5	4.065	1.471	1.562	14.13	19.11	3.315	4.149	2.679	3.183	3037	86.53	65.24
4.0	4.653	1.553	1.630	18.50	25.09	4.047	5.148	3.125	3.699	1.774E+4	165.4	114.6
4.5	5.242	1.615	1.679	23.46	31.89	4.875	6.281	3.565	4.209	1.461E+5	313.7	197.4
5.0	5.830	1.661	1.716	29.00	39.48	5.800	7.549	4.000	4.715	2.266E+6	598.1	337.0

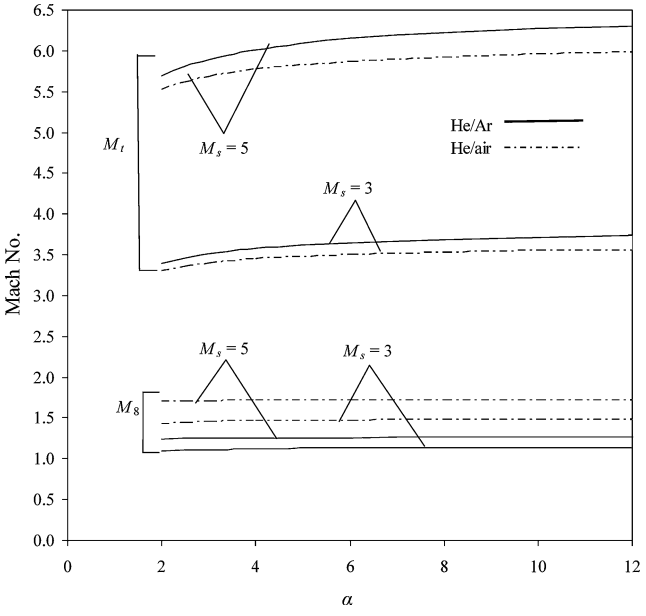

Fig. 2 Variation of M_t and M_8 vs the contraction ratio α.

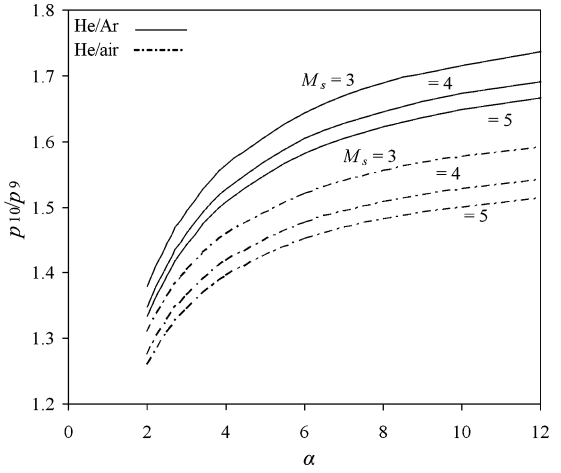

Fig. 3 Variation of p_{10}/p_9 vs the contraction ratio α.

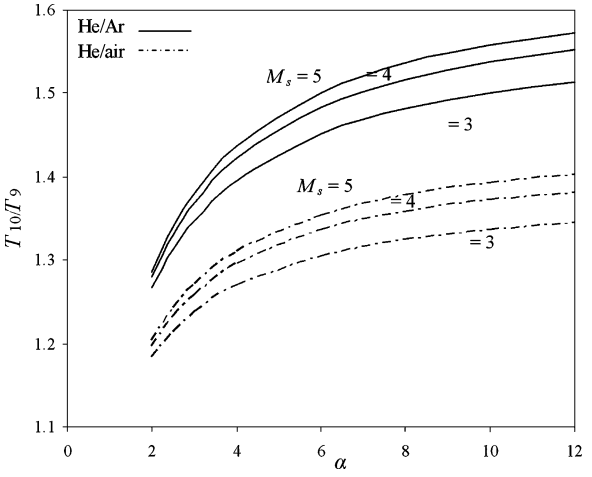

Fig. 4 Variation of T_{10}/T_9 vs the contraction ratio α.

Regions 9 and 10

Region 9 is downstream of the reflected shock when the end of the large-diameter tube is closed. Similarly, region 10 is downstream of the reflected shock in the small-diameter tube (Fig. 1). Equations for these two regions are given at the end of the Appendix.

Results and Discussion

A code was developed based on the foregoing model that is linear in that large loops are not required. The procedure in the code closely follows the order of presentation in the preceding section. Figure 2 shows M_t and M_8 as functions of the contraction ratio when the high-/low-pressure gases are helium/air or helium/argon. The variation in M_t and M_8 with α is slight when α exceeds about 5. This asymptotic behavior holds for other parameters. Thus, an α value of 5 represents a large-area contraction ratio. Table 1 provides parametric results when $\gamma = 1.4$, $\alpha = 5$, and M_s varies from 2.5 to 5.0. The expected increase in M_t over M_s and in $(p, T, w)_8$ over $(p, T, w)_2$ is evident. The percent increase, $(M_t - M_s)10^2/M_s$, slowly increases from 15.64% at $M_s = 2.5$ to 16.59% at $M_s = 5.0$. Note that M_2 is transonic at low M_s values, whereas M_8 is supersonic. Because $\alpha = 5$ in Table 1, M_5 equals 0.1167 for all M_s values.

As already noted, the analysis is independent of the high-pressure gas. The last three columns in Table 1 show p_4/p_1 when the high-/low-pressure gases are air/air, helium/air, and helium/argon, and $T_4 = T_1$. As expected, when the high-pressure gas is air, the diaphragm pressure ratio becomes exorbitant when M_s equals or exceeds 3.5. This is not the case, however, when helium is the high-pressure gas. Note the lower p_4/p_1 pressure ratio for helium/argon compared to helium/air.

Figures 3 and 4 show p_{10}/p_9 and T_{10}/T_9, respectively, for the same high-/low-pressure gases as in Fig. 2. Recall that state 9 is for a conventional shock tube with $T_1 = T_4$. Both the pressure and temperature are enhanced by the contraction, where the rate of increase slows once α exceeds 5. For a given α, p_{10}/p_9 and T_{10}/T_9 have opposite trends as M_s increases. For $\alpha = 5$, helium/argon, and $M_s = 4$, T_{10}/T_9 is 1.46. The T_{10}/T_9 parameter slowly increases with α and M_s. For $\alpha \gg 1$ and $M_s \gg 1$, however, it can reach a value as large as 1.6. Hence, the increase in T_9, relative to T_{10}, is significantly larger than the M_t increase, relative to M_s. A large T_{10} temperature suggests the use of a contraction for radiative heat-transfer studies, high-temperature chemical kinetic and plasma studies, and for high-enthalpy shock-tunnel operation.

Conclusions

A simple, inviscid model is given for a shock tube with a large, abrupt contraction in the low-pressure side. Various limits and constraints are discussed. A unique, nondimensional solution only depends on γ, M_s, and the contraction ratio α. A large α value is 5; above this value there is little change in shock-tube performance. Parametric calculations establish the performance improvement, both behind the transmitted shock and its end-wall reflection.

The performance change stems from the increase in the transmitted shock Mach number relative to a tube without contraction. This performance improvement can be used in conjunction with other performance enhancement techniques.

Appendix: Equations for States 2, 9, and 10

The equations needed for state 2 are

$$p_2/p_1 = [2/(\gamma+1)]Y_s \tag{A1a}$$

$$T_2/T_1 = [2/(\gamma+1)]^2\left(X_sY_s\Big/M_s^2\right) \tag{A1b}$$

$$M_2 = Z_s/(X_sY_s)^{\frac{1}{2}} \tag{A1c}$$

$$R = \bar{R}/W \tag{A1d}$$

$$a_1 = (\gamma RT_1)^{\frac{1}{2}} \tag{A1e}$$

$$w_2/a_1 = [2/(\gamma+1)](Z_s/M_s) \tag{A1f}$$

$$w_s/a_1 = M_s \tag{A1g}$$

$$a_2/a_1 = [2/(\gamma+1)]\left[(X_sY_s)^{\frac{1}{2}}\Big/M_s\right] \tag{A1h}$$

where $X_s = X(M_s)$, and w_s is the large-diameter tube's incident shock speed. The equations for the reflected shock regions, states 9 and 10, are

$$M_{r9} = (Y_s/X_s)^{\frac{1}{2}} \tag{A2a}$$

$$p_9/p_1 = [2/(\gamma+1)](Y_s/X_s)\left\{[(3\gamma-1)/2]M_s^2 - (\gamma-1)\right\} \tag{A2b}$$

$$T_9/T_1 = [2/(\gamma+1)]^2\left(1\Big/M_s^2\right)\left[(\gamma-1)M_s^2 + (3-\gamma)/2\right] \times \left\{[(3\gamma-1)/2]M_s^2 - (\gamma-1)\right\} \tag{A2c}$$

$$M_{r10} = (Y_t/X_t)^{\frac{1}{2}} \tag{A3a}$$

$$p_{10}/p_1 = [2/(\gamma+1)](Y_t/X_t)\left\{[(3\gamma-1)/2]M_t^2 - (\gamma-1)\right\} \tag{A3b}$$

$$T_{10}/T_1 = [2/(\gamma+1)]^2\left(1\Big/M_t^2\right)\left[(\gamma-1)M_t^2 + (3-\gamma)/2\right] \times \left\{[(3\gamma-1)/2]M_t^2 - (\gamma-1)\right\} \tag{A3c}$$

The M_{r9} and M_{r10} Mach numbers are for the respective reflected shock waves that measure the strength of the shocks, that is, they are in a shock-fixed frame.

References

[1]Schneider, S. P., and Haven, C. E., "Quiet-Flow Ludwieg Tube for High-Speed Transition Research," *AIAA Journal*, Vol. 33, No. 4, 1995, pp. 688–693.

[2]Verma, S. B., "Experimental Study of Flow Unsteadiness in a Mach 9 Compression Ramp Interaction Using a Laser Schlieren System," *Measurement Science and Technology*, Vol. 14, No. 7, 2003, pp. 989–997.

[3]Olivier, H., Jiang, Z., Yu, H., and Lu, F. K., "Detonation-Driven Shock Tubes and Tunnels," *Advanced Hypersonic Test Facilities*, edited by F. K. Lu and D. E. Marren, Vol. 198, AIAA, Reston, VA, 2002, pp. 135–203.

[4]Bogdanoff, D. W., "Improvement of Pump Tubes for Gas Guns and Shock Tube Drivers," *AIAA Journal*, Vol. 28, No. 3, 1990, pp. 483–491.

[5]Wilkins, M. E., and Carros, R. J., "Combustion Tests of Oxygen-Hydrogen-Helium Mixtures at Loading Pressures up to 8000 Pounds per Square Inch," NASA TN D-1892, Oct. 1963.

[6]Hiers, R. S., Loubsky, W. J., and Stewart, D. A., "Performance of a Combustion Driven Shock Tunnel with Application to the Tailored-Interface Operating Conditions," NASA TM X-54960, Dec. 1964.

[7]Itoh, K., Ueda, S., Komura, T., Sato, K., Takahashi, M., Miyajima, H., Tanno, H., and Muramoto, H., "Improvement of Free Piston Driver for High Enthalpy Shock Tunnel," *Shock Waves*, Vol. 8, No. 4, 1989, pp. 215–233.

[8]Sharma, S. P., and Park, C., "Operating Characteristics of a 60- and 10-cm Electric Arc Driven Shock Tube—Part I: The Driver," *Journal of Thermophysics and Heat Transfer*, Vol. 4, No. 3, 1990, pp. 259–265.

[9]Belanger, J., and Hornung, H. G., "A Combustion Driven Shock Tunnel to Complement the Free Piston Shock Tunnel T5 at GALCIT," AIAA Paper 92-3968, 1992.

[10]Bogdanoff, D. W., Zambrana, H. A., Cavolowsky, J. A., Newfield, M. E., Cornelison, C. J., and Miller, R. J., "Reactivation and Upgrade of the NASA Ames 16 Inch Shock Tunnel: Status Report," AIAA Paper 92-0327, 1992.

[11]Eitelberg, G., "First Results of Calibration and Use of the HEG," AIAA Paper 94-2525, 1994.

[12]Neely, A. J., and Morgan, R. G., "The Superorbital Expansion Tube Concept, Experiment and Analysis," *Aeronautical Journal*, Vol. 98, No. 973, 1994, pp. 97–105.

[13]Chue, R. S. M., Tsai, C. Y., Bakos, R. J., Erdos, J. I., and Rogers, R. C., "NASA's HYPULSE Facility at GASL—A Dual Mode, Dual Driver Reflected-Shock/Expansion Tunnel," *Advanced Hypersonic Test Facilities*, edited by F. K. Lu and D. E. Marren, Vol. 198, Progress in Astronautics and Aeronautics, AIAA, Reston, VA, 2002, pp. 29–71.

[14]Holden, M. S., and Parker, R. A., "LENS Hypervelocity Tunnels and Application to Vehicle Testing at Duplicated Flight Conditions," *Advanced Hypersonic Test Facilities*, edited by F. K. Lu and D. E. Marren, Vol. 198, Progress in Astronautics and Aeronautics, AIAA, Reston, VA, 2002, pp. 73–110.

[15]Harwell, K. E., and Jahn, R. G., "Initial Ionization Rates in Shock-Heated Argon, Krypton, and Xenon," *Physics of Fluids*, Vol. 7, No. 2, 1964, pp. 214–222.

[16]Johnson, J. A., III, Lin, I., and Santiago, J. P., "Turbulent Collisional Ionising Shock Waves in Argon," *Journal of Physics D: Applied Physics*, Vol. 23, No. 3, 1990, pp. 662–672.

[17]Bogdanoff, D. W., and Park, C., "Radiative Interaction Between Driver and Driven Gases in an Arc-Driven Shock-Tube," *Shock Waves*, Vol. 12, No. 3, 2002, pp. 205–214.

[18]Alpher, R. A., and White, D. R., "Flow in Shock Tubes with Area Change at the Diaphragm Section," *Journal of Fluid Mechanics*, Vol. 3, 1958, pp. 457–470.

[19]Salas, M. D., "Shock Wave Interaction with an Abrupt Area Change," NASA TP 3113, Aug. 1991.

[20]Emanuel, G., *Gasdynamics: Theory and Applications*, AIAA, New York, 1986.

[21]Emanuel, G., *Analytical Fluid Dynamics*, 2nd ed., CRC Press, Boca Raton, FL, 2001, Secs. 12.4 and 12.5.

M. Sichel
Associate Editor